Morphology-controlled preparation of tungsten oxide nanostructures for gas-sensing application*

Qin Yu-Xiang(秦玉香)†, Liu Chang-Yu(刘长雨), and Liu Yang(柳 杨)

School of Electronics and Information Engineering, Tianjin University, Tianjin 300072, *China*

(Received 16 June 2014; revised manuscript received 11 September 2014; published online 10 December 2014)

A novel three-dimensional (3D) hierarchical structure and a roughly oriented one-dimensional (1D) nanowire of WO_3 are selectively prepared on an alumina substrate by an induced hydrothermal growth method. Each hierarchical structure is constructed hydrothermally through bilateral inductive growth of WO_3 nanowire arrays from a nanosheet preformed on the substrate. Only roughly oriented 1D WO_3 nanowire can be obtained from a spherical induction layer. The analyses show that as-prepared 1D nanowire and 3D hierarchical structures exhibit monoclinic and hexagonal phases of WO_3, respectively. The gas-sensing properties of the nanowires and the hierarchical structure of WO_3, which include the variations of their resistances and response times when exposed to NO_2, are investigated at temperatures ranging from room temperature (20 °C) to 250 °C over 0.015 ppm–5 ppm NO_2. The hierarchical WO_3 behaves as a p-type semiconductor at room temperature, and shows p-to-n response characteristic reversal with the increase of temperature. Meanwhile, unlike the 1D nanowire, the hierarchical WO_3 exhibits an excellent response characteristic and very good reversibility and selectivity to NO_2 gas at room temperature due to its unique microstructure. Especially, it is found that the hierarchical WO_3-based sensor is capable of detecting NO_2 at a ppb level with ultrashort response time shorter than 5 s, indicating the potential of this material in developing a highly sensitive gas sensor with a low power consumption.

Keywords: tungsten oxide, gas sensor, hierarchical structure, hydrothermal synthesis

PACS: 73.61.Cw, 07.07.Df, 81.07.Bc, 91.67.Jk **DOI:** 10.1088/1674-1056/24/2/027304

1. Introduction

Detection of toxic gases such as NO_x, O_3, NH_3, and H_2S is important for both environmental protection and human health. Tungsten oxide, which is a wide band-gap n-type semiconductor, has been found to show very promising sensing properties to many toxic and dangerous gases.[1–4] Its sensing mechanism relies on the modulation of electrical conductivity due to surface oxidation or reduction caused by gas exposure. Therefore, the sensitivity is highly dependent on the surface-to-volume ratio of the material, which is further determined by the microstructure and morphology.[5,6] Towards this end, various nanostructures such as nanowires,[7,8] nanotubes,[9] nanorods,[10] and nanoparticles[11] each with a large specific surface area, have been examined as ideal candidates to achieve high gas sensitivity. However, nano-scale materials easily aggregate to form large and dense secondary aggregates (larger particles or thicker bundles) due to the strong and inevitable van der Waals attraction. Such an aggregation results in a considerable decrease in the active surface area and difficult diffusion of gas molecules in sensing films. The agglomeration becomes more serious when the sensor operates at high temperature. In this aspect, how to keep structure stability of the low-dimensional oxides is primarily crucial.

Hierarchical structure, composed of nanostructured building blocks (particles, rods, wires, or sheets), is receiving more and more attention due to its well-developed porous texture and less-agglomerated feature; it is considered to be very attractive for an efficient gas sensor with high sensitivity and a rapid response–recovery characteristic.[12] To date, different hierarchical structures, such as the nanosheets-assembled SnO_2 microsphere,[13] nanorods-assembled $ZnSnO_3$ hollow microsphere,[14] and nanosheets-constructed WO_3 microsphere,[15] have been reported to exhibit exciting results in gas sensitivity and response speed. In this work, we report an induced hydrothermal growth route to actualizing the controlled preparation of a novel nanowire array-assembled hierarchical structure of WO_3. The 3D hierarchical structure or roughly oriented 1D nanowires can be selectively formed by employing an induction layer with the morphology of nanosheets or nanospheres. The microstructure and the assembly mechanism of the as-prepared sample are investigated. Further, the NO_2-sensing properties are evaluated and analyzed. It is found that the hierarchical WO_3 can exhibit high sensitivity and ultrafast response at room temperature due to its unique microstructure feature.

2. Experiments

Nanostructured WO_3 films were *in situ* prepared on alumina substrates coated with a thin tungsten oxide induction layer via a hydrothermal method. The induction layer was pre-

*Project supported by the National Natural Science Foundation of China (Grant Nos. 61274074 and 61271070) and the Natural Science Foundation of Tianjin, China (Grant No. 11JCZDJC15300).

†Corresponding author. E-mail: qinyuxiang@tju.edu.cn

© 2015 Chinese Physical Society and IOP Publishing Ltd

formed on the interdigitated Pt electrodes-attached substrate by spin coating of the precursor solution, followed by thermal annealing. In the experiment, to investigate the effect of an induction layer on the microstructure of WO_3 film, the precursor solution was prepared from sodium tungstate hydrate ($Na_2WO_4{\cdot}2H_2O$) and tungsten hexachloride (WCl_6), respectively.

For the preparation of Na_2WO_4 precursor solution, 2.5-g $Na_2WO_4{\cdot}2H_2O$ and 1-g KCl were co-dissolved in 15-ml deionized water under magnetic stirring. Then 3-ml HCl solution (37 wt%) was added dropwise into the above solution to form a milky suspension. After heating the suspension to 40 °C, 2-ml H_2O_2 was further added under vigorous stirring to obtain the yellow precursor solution. To prepare the induction layer, the above as-prepared precursor solution was spin-coated onto a cleaned alumina substrate with the attached electrodes, and subsequently, the wet substrate was baked at 80 °C for 10 min in a drying oven. During spin coating, a physical mask was used to avoid any residual solution appearing at the end of the electrodes. The above spin-coating and baking procedures were repeated four times to ensure a uniform distribution and adequate coverage of the nanocrystal particles on the substrate. Finally, the obtained substrate was annealed at 550 °C in ambient atmosphere for 1 h to transform the precursor into oxide particles. For the preparation of the induction layer from WCl_6 precursor, 0.4-g WCl_6 and 0.3-g P123 were co-dissolved in 10-ml ethanol under magnetic stirring. After stirring for 30 min, the formed transparent sol-solution served as a precursor solution. Then this solution was spin-coated, baked, and annealed as described above.

In the following step, nanostructured WO_3 was synthesized on the induction layer-coated alumina substrates in the same hydrothermal solution. Firstly, 6-g $Na_2WO_4{\cdot}2H_2O$, 0.4-g P123 surfactant, and 2-g KCl were co-dissolved in 160-ml deionized water under magnetic stirring. Then, the pH value of the mixed solution was adjusted to 2.1$\sim$ 2.5 with a proper volume of HCl (37 wt%). This solution was further aged for about 15 min at room temperature before performing the hydrothermal process. After submerging and sealing the induction layer-coated substrates in the above solution in a 200-ml Teflon-line autoclave, the hydrothermal reaction was conducted at 180 °C for 9 h in an electric oven. Then the autoclave was cooled naturally to room temperature, and the substrates with products were washed several times with deionized water and ethanol, respectively. Finally, the substrates were dried at 80 °C for 5 h at ambient atmosphere. The resulting samples were directly used as sensors to carry out the sensing performance evaluation.

The morphologies and crystalline structures of nanostructured WO_3 films were characterized using a field emission scanning electron microscope (FESEM, Hitachi S-4800), an x-ray diffractometer (XRD, RIGAKU D/MAX 2500 V/PC, Cu Kα radiation) and a field emission transmission electron microscope (FETEM, TECNAI G^2F-20).

The gas-sensing properties of the as-prepared nanostructured WO_3 films were evaluated in a home-built static gas-sensing characterization system,[16] which is equipped in a humidity-controlled testing room. Pure NO_2 gas was injected into the glass test chamber directly to obtain the desired concentration. The operating temperature was changed from room temperature to 250 °C by adjusting the temperature controller of the heating plate. A UNI-T UT61E professional digital multimeter with the function of measuring range automatic adjustment was employed to continuously monitor the resistance change of the sensor in the whole measurement process. The sampling interval was set to be 1 s. During the measurement, the ambient relative humidity is about 30%–35% and the room temperature is about 20 °C.

3. Results and discussion

3.1. Structure characterization

In this work, controlled preparation of 1D or hierarchical WO_3 film on the sensor substrate is realized via a hydrothermal method with the aid of a preformed tungsten oxide induction layer. It is found that using the precursor solution and the particle shape of the annealed induction layer are crucial for the formation of tungsten oxide with different structures. Figures 1(a) and 2(b) show the typical morphologies of the as-synthesized tungsten oxide films from the induction layers resulting from WCl_6 and $Na_2WO_4{\cdot}2H_2O$, respectively. Clearly, very different 1D and hierarchical structures are formed under the same hydrothermal environment. It is therefore assumed that the characteristic of the induction layer plays a decisive role in controlling the final microstructure of the tungsten oxide film after hydrothermal reaction. The insets in Figs. 1(a) and 1(b) illustrate the SEM images of the induction layers formed from the precursors of WCl_6 and $Na_2WO_4{\cdot}2H_2O$, exhibiting the stacked nanospheres and nanosheets respectively. It is believed that the different morphology of the inductive crystal grains is related to the different reaction mechanisms of hydrolysis or decomposition from the precursor of WCl_6 or $Na_2WO_4{\cdot}2H_2O$,[17,18] and then determines the distinctly different microstructure of tungsten oxide. We can see that after a 9-hour hydrothermal reaction at 180 °C, a roughly oriented nanowire carpet is formed on the spheroidal particle-based induction layer (Fig. 1(a)). Adjacent single nanowires assemble together to form bundles with diameters of about 80 nm–120 nm. While based on the nanosheet-like induction layer, a completely different hierarchical structure is observed instead, which is shown in Fig. 1(b). The well-oriented 1D nanowire arrays grow vertically from both sides of the cen-

tral nanosheets, constructing a kind of 3D hierarchical structure film. Figure 1(c) further shows the high-magnification FESEM image of an individual hierarchical structure. It can be seen clearly that the constituent of nanowire shows a very small diameter of about 20 nm and the central nanosheet has a thickness of about 10 nm. This ultrathin feature of the constituents is very favorable for achieving high sensitivity when exposed to a detected gas.

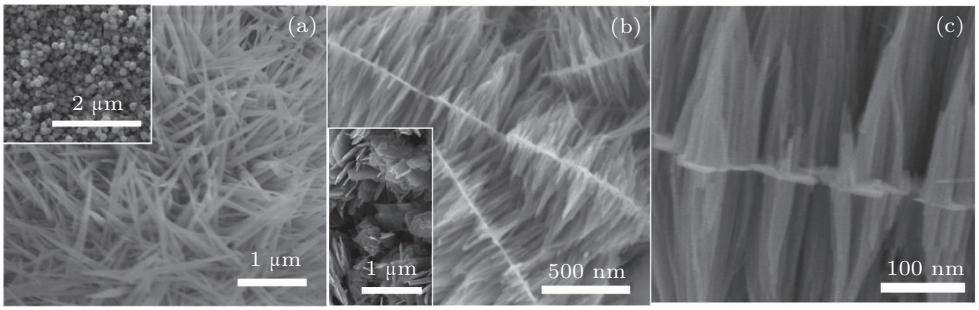


Fig. 1. FESEM images of the as-synthesized tungsten oxides after hydrothermal reaction of 9 h, showing (a) the 1D nanowire carpet on the induction layer resulting from WCl_6, ((b) and (c)) the 3D hierarchical structure on the induction layer resulting from $Na_2WO_4{\cdot}2H_2O$. The insets in panels (a) and (b) respectively show the morphologies of the used induction layers.

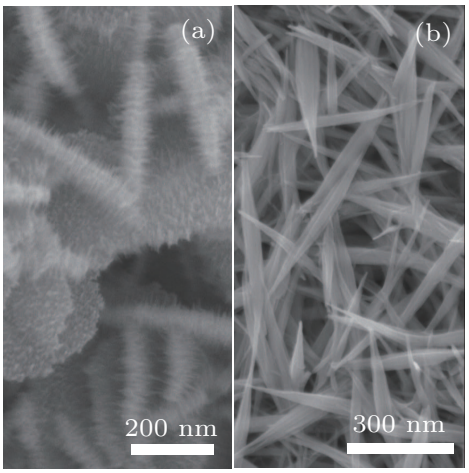


Fig. 2. (a) FESEM images of the intermediate product of the 3D hierarchical structure formed after a 4-hour reaction and (b) the pure nanowires network formed on the bare substrate.

To achieve a more intuitive insight into the role of the induction layer, and to understand the possible growth process of tungsten oxide clearly, figure 2(a) presents the morphology of the intermediate product formed on the nanosheet-like induction layer after a 4-hour hydrothermal reaction. It can be observed that many short and ultrathin nanorods grow vertically from both surfaces of the nanosheets to transform into an integrated hierarchical structure. Extending the reaction time to 9 h results in the double-sided compact nanowire arrays with longer length and larger diameter (Fig. 1(b)). It therefore can be deduced that the double surfaces of the nanosheets provide multiple initial nucleation sites to inspire the preferential aggregation of the tungsten oxide nuclei formed in the hydrothermal solution. The inductive nanosheets serve as the architectural rachises to guide the subsequent self-organization of the 3D hierarchical structures. The induction of the spheroidal grain resulting from WCl_6 can be embodied from the rough orientation of the nanowire carpet from the precoated substrate. Otherwise, only an unordered nanowire bundle network is formed on the bare substrate as presented in Fig. 2(b). The powder centrifuged from the hydrothermal solution exhibits a similar disordered morphology, further indicating the inductive role of the preformed grains for hydrothermal growth of tungsten oxide described above.

The phases of the 1D nanowire carpet and 3D hierarchical structure of tungsten oxide are investigated by the XRD technique, and the results are shown as the solid patterns in Figs. 3(a) and 3(b) respectively. To eliminate the diffraction effect of the substrate materials, the samples were scraped from the alumina substrate for XRD analysis. The strong and sharp diffraction peaks in the figure indicate that the as-developed nanowires and hierarchical structure are highly crystalline. However, the two samples show entirely different XRD patterns evidenced by the discrepancy of diffraction peaks in 2θ position and intensity, indicating completely different crystalline structures. The main diffraction peaks of 1D nanowires developed from the spheroidal induction layer resulting from WCl_6 can be well indexed to the monoclinic phase of WO_3 (JCPDS 43-1035). The strongest peak intensity of the (002) plane indicates that the growth of the nanowire is preferentially along the *c* axis, i.e., the [001] direction. For the 3D hierarchical structure formed from inductive nanosheets, all typical diffraction peaks are well indexed to the profile of hexagonal WO_3 (h-WO_3) (JCPDS 33-1387). The strongest peak of plane (001) implies that the main building blocks of nanorods grow preferentially along the same *c*-axis direction. The high-resolution (HR) TEM images of a single nanowire from the carpet and from the 3D hierarchical structure are respectively shown in Figs. 4(a) and 4(b). Here, the lattice spacings for the two nanowires are 0.384 nm and 0.390 nm, respec-

tively, which perfectly fit the distances of (001) planes of monoclinic WO_3 ($d_{001} = 0.384$ nm, JCPDS 43-1035) and h-WO_3 ($d_{001} = 0.3899$ nm, JCPDS 33-1387). The results indicate that the nanowires from the two samples consist, respectively, of monoclinic and hexagonal WO_3, and their dominant growth directions are along the c-axis direction, which is in agreement with the XRD results.

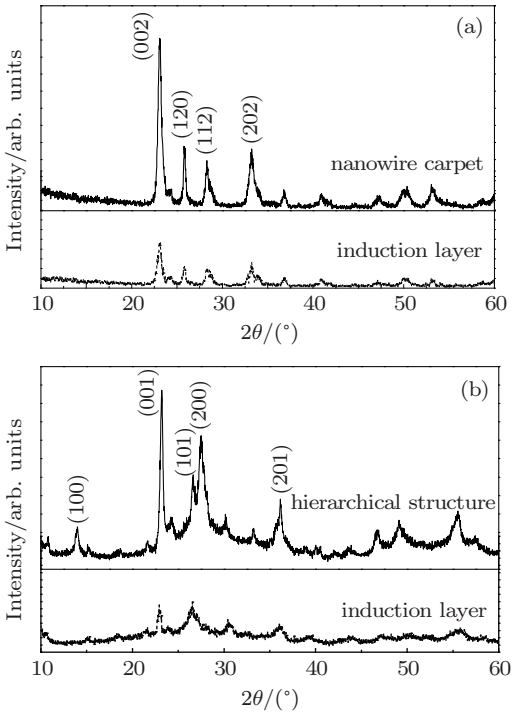


Fig. 3. XRD patterns of induction layers (broken line) and the corresponding hydrothermal products (solid line), showing (a) the induction layer resulting from WCl_6 and the resulting 1D nanowire carpet, and (b) the induction layer resulting from $Na_2WO_4{\cdot}2H_2O$ and the resulting 3D hierarchical structure.

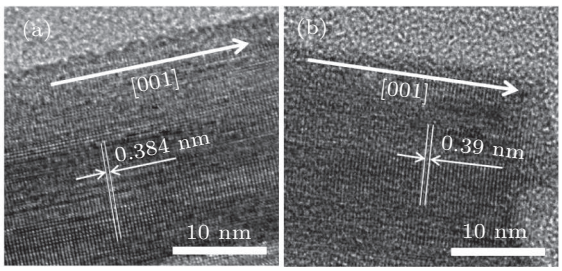


Fig. 4. HRTEM images of a single nanowire from (a) the carpet and (b) the 3D hierarchical structure respectively.

The phase difference between WO_3-synthesized 1D nanowires and 3D hierarchical structures under the same hydrothermal environment give us a much deeper understanding about the key role of the induction layer. The broken line patterns in Figs. 3(a) and 3(b) present the XRD results of the nanospheres and nanosheets induction layers resulting from the precursors of WCl_6 and $Na_2WO_4{\cdot}2H_2O$ respectively. Apparently, the as-developed 1D nanowire or 3D hierarchical structure exhibits the same monoclinic or hexagonal crystalline phase as the original induction layer. That is, the phase of induction layer is decisive to that of the hydrothermal product. In this work, the harvested stable monoclinic or hexagonal phase of WO_3 is assumed to be directly related to the components of the precursor used. As is well known, h-WO_3 is metastable and can transform into monoclinic WO_3 at an appropriate temperature. The structure of h-WO_3 cannot be maintained without some stabilizing ions or molecules in its hexagonal channels.[19] Meanwhile, it is found that alkaline (Na^+, K^+, Cs^+, etc.) or NH_4^+ ions can enter the hexagonal channels of crystallites and effectively block the thermodynamically favored hexagonal–monoclinic transformation.[20] Thus, we believe that the introduced K^+ plays a crucial role in stabilizing the hexagonal structure of the h-WO_3 induction layer during the annealing of the $Na_2WO_4{\cdot}2H_2O$ precursor layer. For the induction layer prepared from the precursor of WCl_6, thermal annealing at 550 °C may result in the stable phase of monoclinic WO_3 due to the absence of K^+ in the precursor solution.

3.2. Gas-sensing properties

The gas-sensing properties are investigated by measuring the changes of resistance of the sensors, before and after introducing the detected gas. Figure 5 shows the relationships between sensor response and operating temperature for the roughly oriented nanowire carpet and 3D hierarchical structure of WO_3 to the NO_2 gas with a flow rate of 1 ppm. Here, the sensor response is defined as $S = R_a/R_g$, where R_a and R_g are the resistances of the sensor in ambient air and in NO_2 gas, respectively. It is observed that unlike the case of 1D nanowires, the response of the hierarchical WO_3 to NO_2 is larger than 1 when the operating temperature is not higher than 50 °C, which means that the resistance of the sensor decreases upon exposure to NO_2 gas. In general, WO_3 is a kind of n-type semiconductor. When it is exposed to oxidizing NO_2 gas, the oxygen of the adsorbed NO_2 acts as an acceptor to extract electrons from the conduction band of the oxide, resulting in the increase of the resistance of WO_3.[21–23] This is the case where the WO_3 nanowire carpet evidences a sensor response smaller than 1 in Fig. 5. In contrast, the hierarchical WO_3 developed here shows an abnormal p-type semiconductor behavior in a low operating temperature range, and a p-to-n-type conductivity transition occurs when the operating temperature is raised to nearly 100 °C. Similar transitions from p- to n-type response (or *vice versa*) resulting from the operating temperature or the gas concentration have been observed for other oxide semiconductors exposed to different gases.[24–27]

The abnormal decrease of resistance for the hierarchical WO_3 upon exposure to oxidizing NO_2 gas at low temperature cannot be explained by using the conventional space charge model. Currently, the origin of the p–n transition is still unclear. Different mechanisms, such as temperature

or gas concentration-caused different surface reactions,[24,25] oxygen adsorption-induced inversion layer,[26,28] and different motilities of carriers,[29] have been suggested. For tungsten oxide with a surface-controlled gas-sensing mechanism, we think, a reasonable explanation about the anomalous p-type response of the hierarchical WO_3 may be made from the theory of surface inversion accompanied with its unique microstructure characteristic. It has been found that 1D nanomaterials favor a larger quantity of dangling bonds and surface defects of oxygen vacancy due to the high surface-to-volume ratio.[30] Moreover, the foreign ions (K^+ here) in WO_3 crystal may introduce additional surface states, serving as evidence of a band of surface states energetically appearing inside the semiconductor band gap.[31] Thus the surface of the hierarchical WO_3 crystal constructed with ultrathin nanowires and nanosheets is expected to be very active to induce very strong absorption of oxygen even at low temperature due to the large density of surface states. The strong oxygen adsorption significantly increases the depletion region inside the oxide surface and upward band bending, causing an inversion layer with the p-type feature (the Fermi level E_F lies below the intrinsic level E_i) instead of a depletion layer created by normal surface adsorption.[28] The strong ability of surface adsorption of the hierarchical WO_3 induced by its ultrathin constituents and the additive of K^+ also explains its remarkably sensitive performance exhibiting at room temperature. As the operating temperature increases, a larger number of electrons jump into the conduction band from the valence band, resulting in the transition from p- to n-type at a certain temperature.[28]

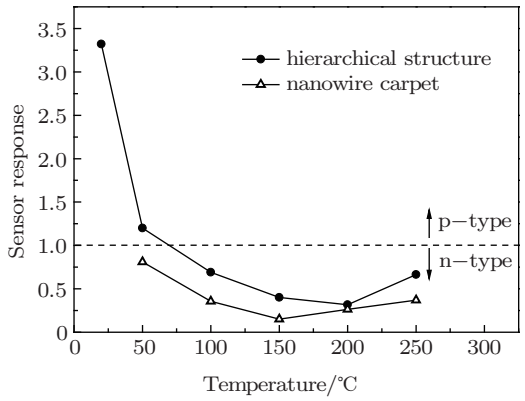


Fig. 5. Relationships between sensor response and operating temperature for the roughly oriented nanowire carpet and hierarchical structure of WO_3 to 1-ppm NO_2 gas.

Comparatively, the sensor based on the monoclinic WO_3 nanowire carpet shows a normal p-type response characteristic under the whole operating temperature range. At room temperature, however, only a very poor response (1.05, $S = R_g/R_a$) to 1-ppm NO_2 is observed. We think it might be partially related to the bundle-like morphology of the nanowires, which can hamper the gas diffusion toward the sensing surface located inside the bundles.

Figure 6 shows the dynamic responses of the hierarchical WO_3 film-based sensor to varying concentrations of NO_2 gas at room temperature. As can be seen, the measured resistances decrease upon exposure to oxidizing NO_2 gas, showing a p-type semiconductor behavior. Notably, the as-developed hierarchical WO_3 film is responsive to very dilute NO_2 (15 ppb) at room temperature. It indicates that this hierarchical WO_3-based sensor is indeed capable of NO_2 detection at the ppb level even under room temperature conditions, which is still a big challenge to conventional sensing materials. At room temperature, the sensor resistances could recover to its initial value after NO_2 removal. Even after four response-recovery cycles to different NO_2 concentrations (0.015 ppm–5 ppm), there is almost no obvious change between recovered resistance and baseline resistance, indicating a good reversibility.

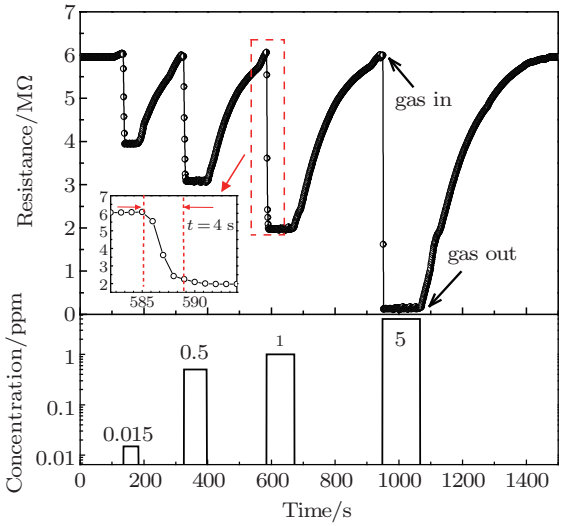


Fig. 6. (color online) Dynamic responses of the hierarchical WO_3 films-based sensor to varying concentrations of NO_2 gas at room temperature.

Another noteworthy characteristic for the hierarchical WO_3-based sensor is the ultrafast response exhibiting at room temperature. It is observed from Fig. 6 that the sensor resistance shows a rapid change upon exposure to NO_2 gas with concentrations from the ppb to the ppm level. The 90% of response times (the response time t_{res}, is the time that is required for the sensor resistance to reach 90% of its equilibrium value after the test gas has been injected) for the hierarchical WO_3 sensor are no more than 5-s upon exposure to 0.015 ppm–5 ppm NO_2, exhibiting a unique ultrafast response characteristic. The inset in Fig. 6 shows the enlarged response curve of the hierarchical WO_3-based sensor to 1-ppm NO_2 gas. The above ultrafast response characteristic could hardly be achieved from 1D nanostructured oxide-based sensors at room temperature. For the sensors based on the WO_3 nanorod and nanowire, the reported response times are usually above one hundred seconds to 0.5 ppm–2 ppm NO_2 at their optical working temperature of 200 °C.[32,33]

It seems that the unique NO_2-sensing properties of the hierarchical WO_3-based sensor at room temperature may be ascribed to the characteristic architecture of the double-sided assembly of well-aligned nanowire arrays. For a gas sensor, the efficient utilization of the surface area and surface accessibility is crucial to maintain the high sensitivity and fast response characteristic.[12] At a given temperature, gas diffusion can be considered to be a primary factor that determines the gas response kinetics.[34] For the WO_3 hierarchical structure developed from an inductive nanosheet, the ultrathin feature of the 1D nanowire constituents ensures that the large active area interacts with the gas molecules. Meanwhile, the well-aligned arrays make NO_2 molecules diffuse agilely in the sensing layer. These features are assumed to result in the ultrafast response as well as the high response value when exposed to detected gas. On the other hand, for the hierarchical WO_3, the K^+ introduced in the crystal is expected not only to stabilize the hexagonal structure of h-WO_3 but also to act as dopants to improve the sensitivity of the oxide sensor at low temperature effectively.[35]

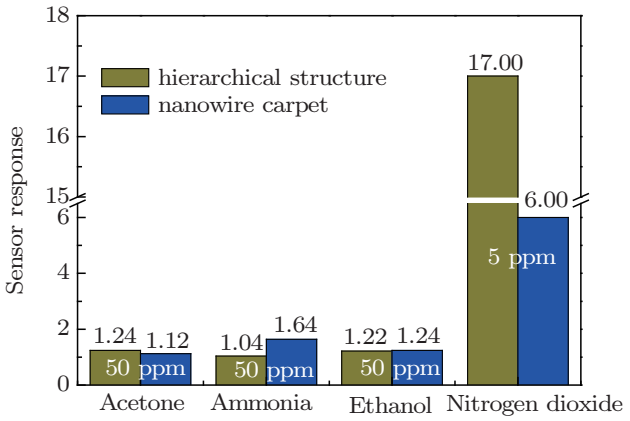


Fig. 7. (color online) Responses of the WO_3 sensor based on the 1D nanowire carpet and the 3D hierarchical structure to different gases at room temperature.

The selective capacity is very important for the practical application of a gas sensor. In order to evaluate the selectivity of the as-developed WO_3 sensor based on the nanowire carpet and hierarchical structure, the gas responses of both sensors to NH_3, acetone, and ethanol with the same concentration of 50 ppm are also respectively tested at room temperature and further compared with the response to 5-ppm NO_2, which are shown in Fig. 7. Here, the sensor response is calculated by R_g/R_a or R_a/R_g, to ensure that the response values are always not smaller than 1. It can be seen that in comparison with the case of NO_2 gas, both WO_3 sensors are insensitive to NH_3 and other two organic gases with evidence of very low response values of 1.04–1.64. However, the discrepancy in selectivity between both sensors appears to be significant. As shown in Fig. 7, the response values to 5-ppm NO_2 for the sensors based on the hierarchical structure and the nanowire carpet are respectively 17 and 6.0 at room temperature. Thus, much better selectivity to NO_2 gas can be expected for the 3D hierarchical WO_3 sensor, which is very promising in developing an NO_2 sensor with low power consumption and high gas selectivity.

4. Conclusions

With the aid of inductive nanosheets or nanospheres preformed on the substrate, a novel 3D hierarchical structure of h-WO_3 and roughly oriented WO_3 nanowires with monoclinic phase are selectively prepared by using a hydrothermal method. The morphology and crystalline structure of the inductive grain, which can be controlled easily by the used precursor solution, are believed to play a decisive role in developing 1D or hierarchical WO_3 with different phases. The individual hierarchical structure is constructed through inductive growth of ultrathin nanowire arrays on the double sides of the central nanosheet, showing a kind of very effective microstructure for gas-sensing application. As a result, the as-prepared hierarchical WO_3 exhibits satisfied sensing properties to NO_2 gas at room temperature, including an excellent response characteristic and good reversibility and selectivity. Note that at room temperature, the hierarchical WO_3-based sensor responses to NO_2 at a ppb level with an ultrafast response characteristic. The response times to 0.015 ppm–5 ppm NO_2 are shorter than 5 s. Comparatively, the roughly oriented nanowires only exhibit a very poor gas response at room temperature. This work demonstrates the potential of the hierarchical structure in developing a high sensitive gas sensor with low power consumption.

References

[1] Lee D S, Nam K H and Lee D D 2000 *Thin Solid Films* **375** 142
[2] Hieu N V, Quang V V, Hoa N D and Kim D 2011 *Curr. Appl. Phys.* **11** 657
[3] Qin Y X, Liu K X and Liu C Y 2013 *Acta Phys. Sin.* **62** 208104 (in Chinese)
[4] Datta N, Ramgir N, Kaur M, Roy M, Bhatt R, Kailasaganapathi S, Debnath A K, Aswal D K and Gupta S K 2012 *Mater. Chem. Phys.* **134** 851
[5] Shen Y B, Yamazaki T, Liu Z F, Meng D, Kikuta T and Nakatani N 2009 *Thin Solid Films* **517** 2069
[6] Ponzoni A, Comini E, Sberveglieri G, Zhou J, Deng S Z, Xu N S, Ding Y and Wang Z L 2006 *Appl. Phys. Lett.* **88** 203101
[7] Huang R, Zhu J and Yu R 2009 *Chin. Phys. B* **18** 3024
[8] Yuan H J, Chen Y Q, Yu F, Peng Y H, He X W, Zhao D and Tang D S 2011 *Chin. Phys. B* **20** 036103
[9] Yang T S, Zhang Y and Li C 2014 *J. Alloys Compd.* **584** 546
[10] Wu Y Q, Hu M and Wei X Y 2014 *Chin. Phys. B* **23** 040704
[11] Meng D, Yamazaki T, Shen Y B, Liu Z F and Kikuta T 2009 *Appl. Surf. Sci.* **256** 1050
[12] Lee J H 2009 *Sens. Actuators B* **140** 319
[13] Kim H R, Choi K I, Lee J H and Akbar S A 2009 *Sens. Actuators B* **136** 138
[14] Bing Y, Zeng Y, Liu C, Qiao L, Sui Y, Zou B, Zheng W and Zou G 2014 *Sens. Actuators B* **190** 370
[15] Bai S, Zhang K, Luo R, Li D, Chen A and Liu C C 2013 *Mater. Lett.* **111** 32

[16] Qin Y X, Hu M and Zhang J 2010 *Sens. Actuators B* **150** 339
[17] Yu Y 2009 "Preparation and Characterization of Mesoporous Tungsten Oxide" (MS Thesis) (Changsha: Central South University) (in Chinese)
[18] Jiao Z H, Sun X W, Wang J M, Ke L and Demir H V 2010 *J. Phys. D: Appl. Phys.* **43** 285501
[19] Szilágyi I M, Madarász J, Pokol G, Király P, Tárkányi G, Saukko S, Mizsei J, Tóth A L, Szabó A and Josepovits V 2008 *Chem. Mater.* **20** 4116
[20] Shen X P, Wang G X and Wexlera D 2009 *Sens. Actuators B* **143** 325
[21] Hua Z, Wang Y, Wang H and Dong L 2010 *Sens. Actuators B* **150** 588
[22] Zhang C, Debliquy M, Boudiba A, Liao H and Coddet C 2010 *Sens. Actuators B* **144** 280
[23] Wang S H, Chou T C and Liu C C 2003 *Sens. Actuators B* **94** 343
[24] Zhang C, Debliquy M, Boudiba A, Liao H and Coddet C 2010 *Sens. Actuators B* **144** 280
[25] Siciliano T, Tepore A, Micocci G, Genga A, Siciliano M and Filippo E 2009 *Sens. Actuators B* **138** 207
[26] Galatsis K, Cukrov L, Wlodarski W, McCormick P, Kalantar-zadeh K, Comini E and Sberveglieri G 2003 *Sens. Actuators B* **93** 562
[27] Kim Y S, Hwang I S, Kim S J, Lee C Y and Lee J H 2008 *Sens. Actuators B* **135** 298
[28] Gurlo A, Barsan N, Oprea A, Sahm M, Sahm T and Weimar U 2004 *Appl. Phys. Lett.* **85** 2280
[29] Kim Y S, Ha S C, Kim K, Yang H, Park J T, Lee C H, Choi J, Paek J and Lee K 2005 *Appl. Phys. Lett.* **86** 213105
[30] Huang M H, Wu Y Y, Feick H, Tran N, Weber E and Yang P D 2001 *Adv. Mater.* **13** 113
[31] Cabot A, Diéguez A, Romano-Rodriguez A, Morante J R and Bârsan N 2001 *Sens. Actuators B* **79** 98
[32] Ponzonia A, Russo V, Bailini A, Casari C S, Ferroni M, Bassi A L, Migliori A, Morandi V, Ortolani L, Sberveglieri G and Bottani C E 2011 *Sens. Actuators B* **153** 340
[33] Hieu N V, Vuong H V, Duy N V and Hoa N D 2012 *Sens. Actuators B* **171–172** 760
[34] Rossinyol E, Prim A, Pellicer E, Arbiol J, Hernández-Ramírez F, Peiró F, Cornet A, Morante J R, Solovyov L A, Tian B, Bo T and Zhao D 2007 *Adv. Funct. Mater.* **17** 1801
[35] Bai S, Li D, Han D, Luo R, Chen A and Chung C 2010 *Sens. Actuators B* **150** 749